

Phase-engineered transition-metal dichalcogenides for energy and electronics

Manish Chhowalla, Damien Voiry, Jieun Yang, Hyeon Suk Shin, and Kian Ping Loh

Two-dimensional (2D) transition-metal dichalcogenides (TMDs) consist of over 40 compounds. Complex metal TMDs assume the 1T phase where the transition-metal atom coordination is octahedral. The 2H phase is stable in semiconducting TMDs where the coordination of metal atoms is trigonal prismatic. Stability issues have hampered the study of interesting phenomena in two-dimensional 1T phase TMDs. Phase conversion in TMDs involves transformation by chemistry at room temperature and pressure. It is possible to convert 2H phase 2D TMDs to the 1T phase or locally pattern the 1T phase on the 2H phase. The chemically converted 1T phase 2D TMDs exhibit interesting properties that are being exploited for catalysis, source and drain electrodes in field-effect transistors, and energy storage. We summarize the key properties of 2D 1T phase TMDs and their applications as electrodes for energy and electronics.

Phases in transition-metal dichalcogenides

The three phases of semiconducting transition-metal dichalcogenides (TMDs) are shown in **Figure 1**.^{1–6} The thermodynamically stable 2H phase in TMDs is semiconducting and is the trigonal prismatic structure shown in Figure 1a. It is referred to as the 2H phase because the unit cell extends into two basal planes. This convention is also used for monolayered TMDs. The octahedral metal-ion coordinated 1T phase is metallic and is not found in naturally formed minerals because it is recognized as being unstable (Figure 1b). The 1T' phase is a distorted version of the 1T phase (Figure 1c). An additional 3R phase is found only in bulk compounds and relaxes to the 2H phase upon mild heating.⁷

Theoretical calculations have indicated that the 1T phase is inherently unstable and cannot be realized, whereas the 1T' and 2H phases are stable.^{8,9} Experimentally, however, it has been found that the 1T' phase is the least stable and relaxes to the 1T phase that, in turn, relaxes to the most stable 2H configuration (see atomic resolution transmission electron microscopy images in Figure 1e–g).⁴ The 1T phase was realized several decades ago in alkali-metal (Li and K) intercalated TMDs.^{1,2,10,11} Intercalation of TMDs leads to large expansion of the interlayer spacing such

that solvation and reduction of intercalants lead to exfoliation into individual layers.^{2,3,10,12–14} These monolayered nanosheets are composed of a large fraction of the 1T phase.^{5,15}

The conversion of the 2H phase to the 1T phase during intercalation is attributed to charge transfer from the alkali atoms to the nanosheets. This additional charge results in density of states at the Fermi level, rendering the material metallic. More specifically, crystal mean field theory shows that the 2H phase of TMDs such as MoS₂ is semiconducting because of symmetry-induced splitting of the Mo 4*d* orbitals into three groups: the completely occupied Mo 4*d*_{z²} orbital; Mo 4*d*_{xy} and Mo 4*d*_{x²-y²}; and Mo 4*d*_{xz} and Mo 4*d*_{yz} that are unoccupied. The S 3*p* states do not influence the electronic structure of the material, as they are located approximately 3 eV away from the Fermi level. In the case of the 1T phase, the Mo 4*d* orbitals split into two groups: three degenerate Mo 4*d*_{xy,yz,xz} orbitals occupied by two electrons; and the unoccupied Mo 4*d*_{z²} and Mo 4*d*_{x²-y²}. The incomplete occupation of the Mo 4*d*_{xy,yz,xz} orbitals renders the 1T phase metallic but also makes it unstable. Completing the occupation of the Mo 4*d*_{xy,yz,xz} orbitals via additional electrons from dopants stabilizes the 1T phase but destabilizes the 2H phase, thus allowing phase conversion to occur.^{9,16,17}

Manish Chhowalla, Department of Materials Science and Engineering, Rutgers, The State University of New Jersey, USA; manish1@rci.rutgers.edu

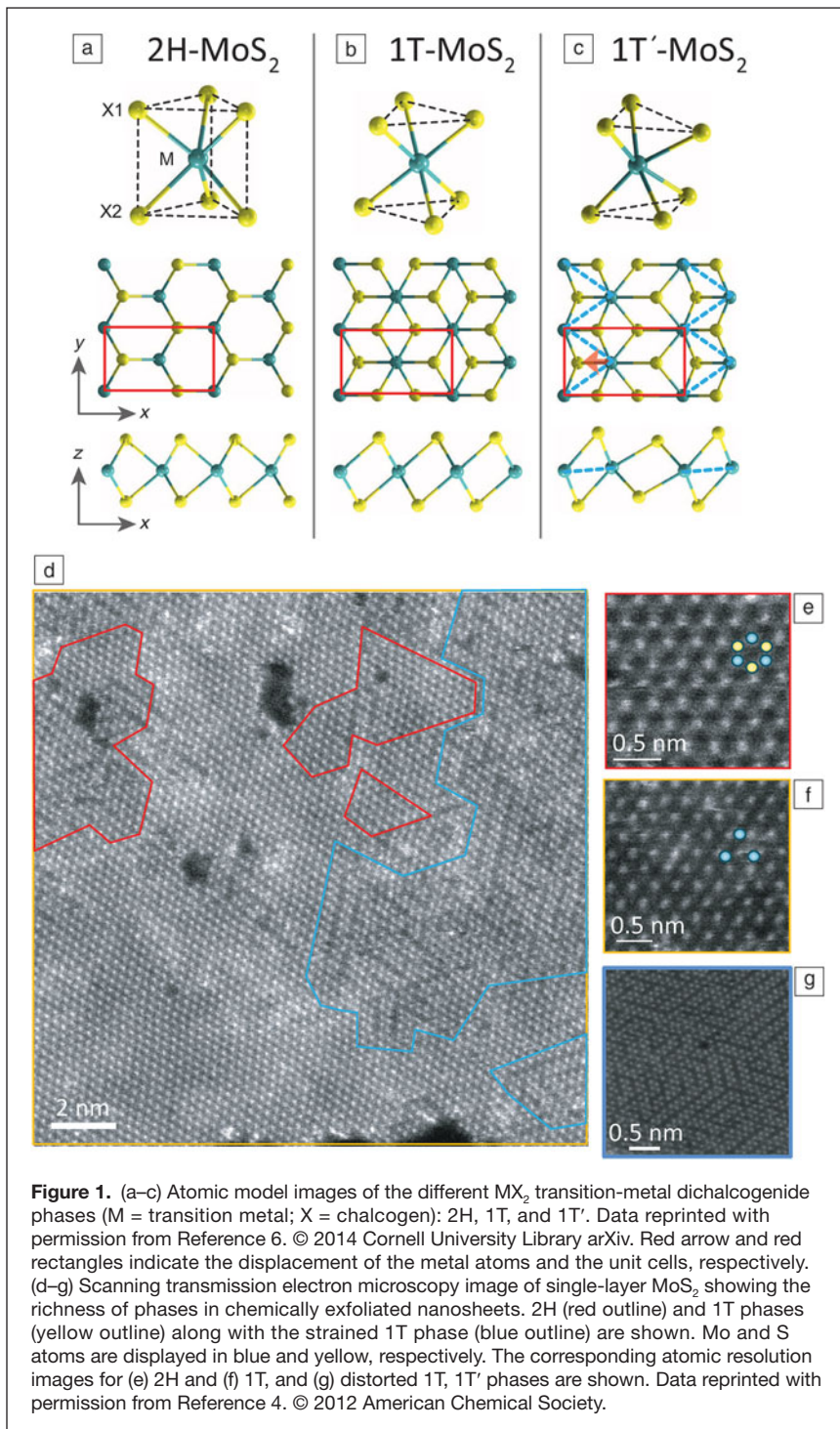
Damien Voiry, Department of Materials Science and Engineering, Rutgers, The State University of New Jersey, USA; damienvoiry@rutgers.edu

Jieun Yang, Department of Materials Science and Engineering, Rutgers, The State University of New Jersey, USA; juliayang411@gmail.com

Hyeon Suk Shin, Department of Chemistry and Department of Energy Engineering, Ulsan National Institute of Science and Technology, South Korea; shin@unist.ac.kr

Kian Ping Loh, Department of Chemistry, National University of Singapore, Singapore; chmlpkp@nus.edu.sg

DOI: 10.1557/mrs.2015.142



In addition to alkali doping via intercalation, substitutional doping with elements with a higher number of valence electrons (e.g., Re, Mn) than transition-metal ions in TMDs can also lead to formation of the 1T phase.¹⁸ Phase transformations have been induced and monitored in real time using transmission electron microscopy.^{19,20} Suenega et al.¹⁹ showed that under appropriate irradiation conditions, it was possible to reversibly induce the 2H, 1T, and 1T' phases in MoS_2 in a

transmission electron microscope. Hot electron injection into MoS_2 nanosheets using plasmon resonance from gold nanoparticles has also claimed to induce reversible phase transformations.²¹ Reed et al. have theoretically demonstrated that strain and strain engineering are important variables in phase transformations of TMDs.²²

Although additional electrons from dopants are required for transformation from the 2H to the 1T phase, the presence of such impurities is undesirable.¹⁹ The removal of dopants should destabilize the 1T phase. In lithium intercalated TMDs (e.g., Li_xMoS_2), butyl lithium is used. The organic butyl and Li ions can be removed from the MoS_2 nanosheets by carefully washing with hexane and water.^{15,23} Surprisingly, the 1T phase remains after removal of the organic and alkali impurities.⁴ “Dry” films of the chemically pure 1T phase TMDs in both multi- and monolayered forms have been demonstrated.⁵ The stability of these films is attributed to the presence of protons or other immobile, positively charged ions on the surface of the nanosheets that counter the additional electronic charge donated by the dopants. The presence of adsorbed, positively charged counter ions on nanosheets is supported by the fact that the 1T phase relaxes to the 2H phase upon annealing to $\sim 300^\circ\text{C}$ in a controlled environment.^{5,15}

The ability to controllably induce different phases of the TMDs has led to both fundamental^{4,6} and technologically relevant^{15,23–25} research aimed at exploiting the unique properties of the phases. Recently, it was discovered that the 1T' phase has unique topological properties that make it applicable for studying novel condensed matter phenomena such as superconductivity.^{26,27} The metallic 1T phase is interesting, because it provides high conductivity for charge transfer in electrochemical processes such as catalysis and energy storage.^{15,25,28–31} The ability to locally engineer the various different phases also allows for patterning heterostructures for electronics. We review some recent work on using TMDs as

electrodes in electronics, for electrochemical charge storage, and catalysis. We highlight recent advances and demonstrate how phase engineering can be utilized for improving the performance of devices incorporating 2D TMDs.

Two-dimensional TMDs for energy storage

Layered TMD materials were first investigated for energy storage applications in the 1970s^{32,33} but were abandoned

due to their poor stability. More recently, electrodes made from restacked TMD nanosheets have gained interest.^{34–38} The restacked nanosheets consist of exfoliated nanosheets assembled in the form of thin films. Such films expand and contract and allow ions to diffuse in and out of the layered structure. Drexel University scientists recently discovered an entirely new family of 2D materials—early transition-metal carbides and carbonitrides called MXenes.^{39–43} These materials are chemically exfoliated from the MAX phases, which are a large family (in excess of 60 members) of hexagonal layered ternary transition-metal carbides and/or nitrides with composition of $M_{n+1}AX_n$, where M stands for an early transition metal (such as Ti, V, Cr, Nb), A stands for a group A element (such as Al, Si, Sn, In), X stands for carbon and/or nitrogen, and $n = 1, 2, \text{ or } 3$. Selective etching of the A-group element from a MAX phase results in the formation of 2D $M_{n+1}X_n$ layers, labeled “MXene.” Very large volumetric capacitance values in excess of $900 \text{ F}\cdot\text{cm}^{-3}$ have been achieved in MXenes,^{39,44} partially because they are highly conducting and hydrophilic.

In the case of 2D TMDs, the electrical conductivity of the 2H phase is too low for good electrodes.^{45,46} Strategies for overcoming the electrical conductivity issue in TMDs for electrochemical charge storage include forming composites with conducting reduced graphene oxide (rGO).^{47,48} Layer-by-layer stacked heterostructures of rGO and 2D TMDs are being increasingly exploited for energy applications in batteries and supercapacitors (**Figure 2**).^{37,38,49–51}

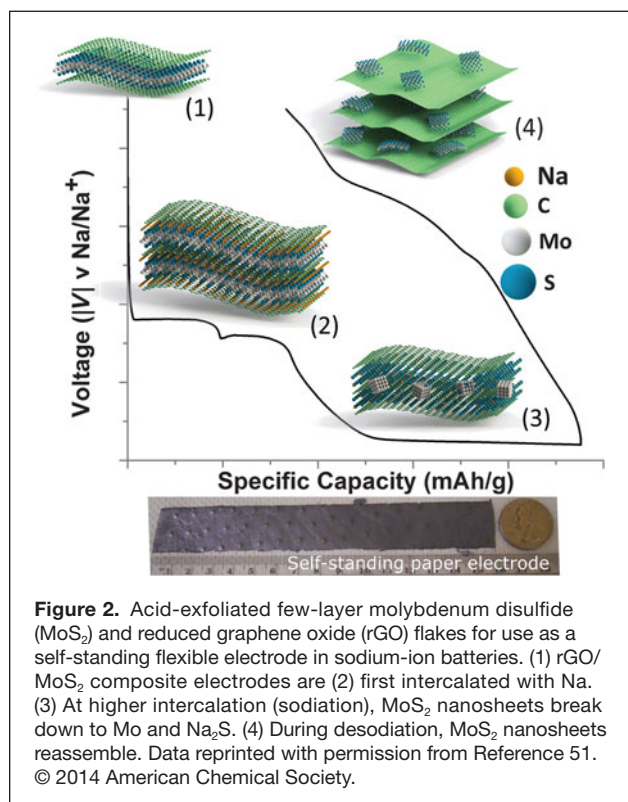
On their own, most 2D TMDs have the ability to store Li^+ at higher capacities than graphene-based anodes; however, they

are chemically unstable when charged electrically and exhibit poor rate performance (i.e., poor capacitance at high charge/discharge rates) and cycle performance (i.e., poor stability of the electrodes).⁵² Besides intercalation, there are potential conversion and oxidation reactions, which must be controlled to allow stable and high rate cycling. When cast in the form of a composite with rGO, synergistic interactions with rGO have been shown to mitigate the inherent instability. Besides acting as a conductive additive, rGO sheets play the role of a scaffolding material preventing direct stacking of the 2D TMDs, thus allowing for an expanded interlayer distance that buffers against volume swings during charge and discharge.⁵³

The emerging large-scale battery market demands low-cost and high-power or high-energy density materials. The niche market for 2D TMDs as energy storage materials may be in alternative anode materials in systems such as the sodium-ion battery, which is attractive because of its low cost and natural abundance. Most negative electrodes in sodium-ion batteries use materials that undergo an alloying reaction with sodium. The advantage of the vertically stacked 2D TMD structures is that its weak interlayer bonding buffers against volume swings during charge and discharge cycles.

Molybdenum disulfide can be a good storage medium for sodium ions, based on a combination of intercalation and a conversion-type reaction.^{36,51,54} Theoretical calculations reveal moderately strong binding between Na and MoS_2 that is thermodynamically favorable against cluster formation and phase separation of Na. Thanks to the lower binding energy between Na and MoS_2 , Na atoms prefer to intercalate in the gap between the MoS_2 layers rather than aggregating in the form of clusters. Intercalation of Na in MoS_2 gives rise to a maximum theoretical capacity of $146 \text{ mAh}\cdot\text{g}^{-1}$ and a low average electrode potential in the range of $0.75\text{--}1.25 \text{ V}$.⁵⁵ If the storage mechanism is based only on intercalation/deintercalation, the obtainable capacity is not impressive. Electrochemical studies reveal, however, that when further discharged to lower voltage (0.01 V), a high capacity reversible conversion reaction can be accessed.

Wang et al. tested an exfoliated $\text{MoS}_2\text{--C}$ composite prepared via chemical exfoliation and hydrothermal reaction (hydrothermal reaction is a synthesis method to produce nanomaterials and crystals from an aqueous solution using high pressure and high temperature); a high capacity of $400 \text{ mA}\cdot\text{h}\cdot\text{g}^{-1}$ at 0.25 C ($100 \text{ mA}\cdot\text{g}^{-1}$) was maintained over prolonged cycling life.⁵⁶ Outstanding rate capability was also achieved with a capacity of $290 \text{ mAh}\cdot\text{g}^{-1}$ at 5 C . The discharge/charge profile of the composite shows voltage hysteresis and slope characteristics that are typical of a conversion reaction. Three plateaus are observed in the galvanostatic discharge, at 0.9 V , 0.73 V , and 0.1 V . The first strongly pronounced plateau at 0.9 V is indicative of the formation of Na_xMoS_2 ; the plateau at 0.73 V is related to further Na ion reaction with MoS_2 ; and the long 0.1 V plateau should be related to the reduction of Mo^{4+} to Mo metal, accompanied by the formation of Na_2S nanoparticles.



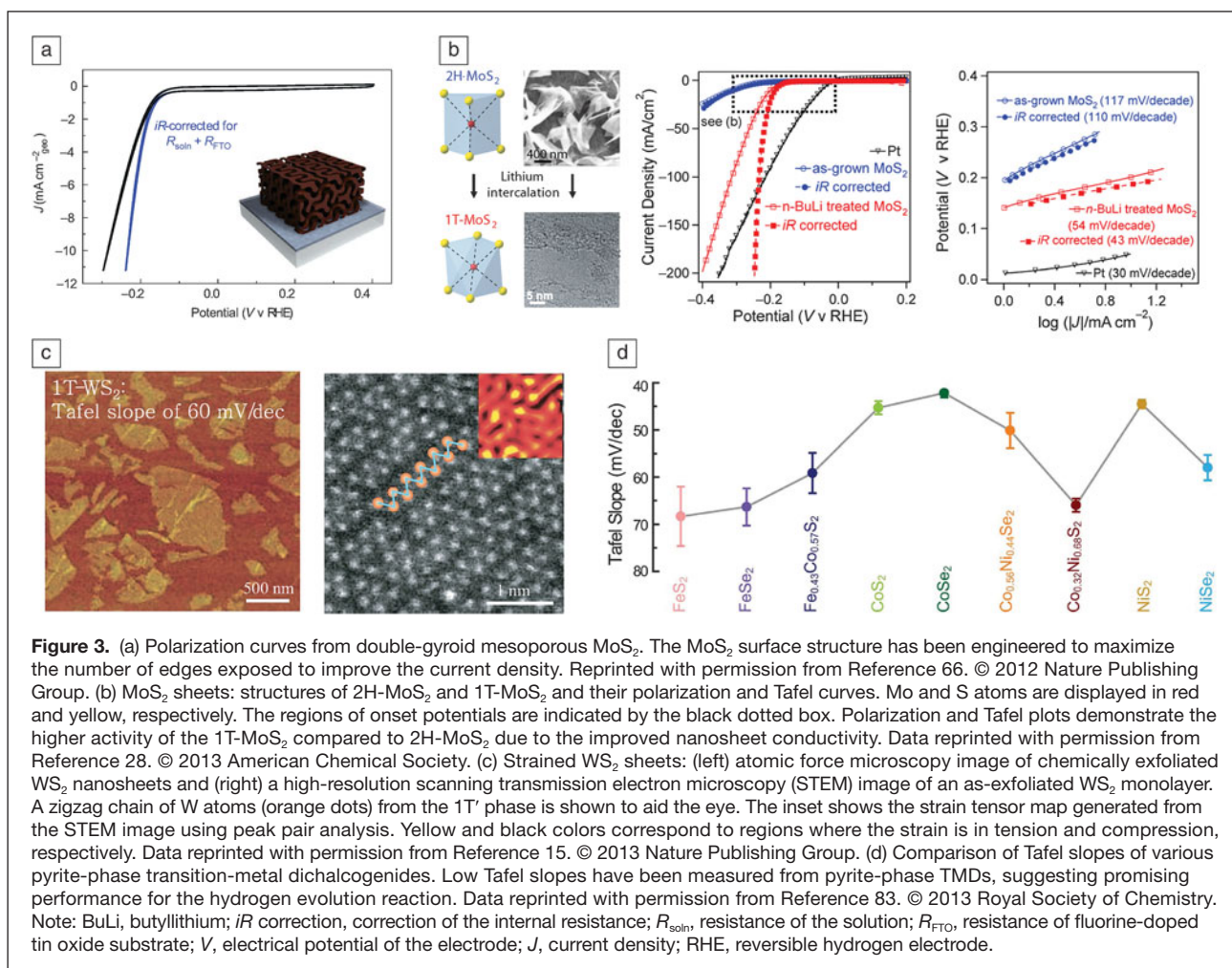
The advantage of 2D TMDs is their ability to be stacked readily to form a paper-like membrane, thus enabling application in flexible batteries. A large-area composite paper (see Figure 2) comprising acid-treated layered MoS_2 and chemically modified graphene in an interleaved structure offers a stable charge capacity of $230 \text{ mAh}\cdot\text{g}^{-1}$ and allows room temperature operation, as opposed to most sodium battery materials that can only operate at temperature $T > 300^\circ\text{C}$.⁵⁷ The interleaved and porous structure of the paper electrode offers smooth channels for sodium to diffuse in and out as the cell is charged and discharged quickly.⁵¹

Flexible supercapacitors are very promising emerging energy storage devices and of great interest, owing to their high-power density with improved mechanical behavior and making them suitable as power backups for future stretchable electronics. Recently, there has been substantial interest in improving the conductivity of 2D TMDs by introducing the 1T phase. Although much of this work is preliminary, 1T phase electrodes made from restacked MoS_2 nanosheets have conductivity values comparable to those for rGO electrodes.⁵⁸ Recent results with VS_2 nanosheets, with its permeable scaffolds, metallic properties, and high oxidation state suggest that

metallic 2D TMDs are particularly amenable to form supercapacitors with in-plane configurations.⁵⁹ A specific capacitance of $4760 \mu\text{F}/\text{cm}^2$ was realized here in an in-plane configuration and a film thickness of 150 nm, of which no obvious degradation was observed even after 1000 charge/discharge cycles. More recent results have shown that the metallic 1T phase electrodes of MoS_2 possess volumetric capacitance values in excess of $600 \text{ F}\cdot\text{cm}^{-3}$ along with energy and power densities comparable to the best performances of rGO electrodes.⁵⁸

TMDs as catalysts for hydrogen evolution reaction

The first report on the hydrogen evolution reaction (HER) activity of bulk MoS_2 was published in 1977.⁶⁰ Since the performance (an onset potential -0.09 V versus reversible hydrogen electrode [RHE] and a Tafel slope of $692 \text{ mV}/\text{dec}$) was not good, MoS_2 was considered to be an inefficient catalyst because of its large internal resistance.^{60,61} Optimal onset potential and Tafel slope should be as low as possible. For example platinum has an onset potential of $<20 \text{ mV}$ and a Tafel of $30 \text{ mV}/\text{dec}$. However, density functional theory calculations by Hinnemann et al. attracted interest because they showed



that the free energy of H adsorption on MoS₂ edge sites was close to that on both hydrogenase and Pt.⁶² Thus, the edges of MoS₂ were considered as active sites in catalysis for H₂ evolution. This was experimentally proven by Chorkendorff et al. using MoS₂ nanoparticles grown on Au (111), which showed high catalytic activity with an onset potential of -0.15 V versus RHE and a Tafel slope of 55–60 mV/dec.⁶³

Since then, several approaches to improve the performance of HER have been explored. The first approach is to enhance the intrinsic catalytic activity of TMDs. An example of this is doping MoS₂ with Co.^{64,65} The second approach is to increase the number of active sites of the catalyst by controlling the surface properties of MoS₂. In some studies, the surface structure of MoS₂ was engineered to preferentially expose edge sites.^{66–68} Jaramillo et al. synthesized a highly ordered double-gyroid MoS₂ bicontinuous network with nanoscale pores (**Figure 3a**).⁶⁶ The basal plane of MoS₂, which has a limited number of active sites, can be overcome by changing the surface structure. This catalyst showed excellent HER activity, with an onset potential of -0.2 to -0.15 V versus RHE and a Tafel slope of 50 mV/dec. Alternatively, MoS₂ and MoSe₂ films can be prepared with vertically aligned layers that expose the edges on the film surface.⁶⁷

The third approach is to increase electron transport from the active sites to the electrode. Graphene-based TMD hybrids have demonstrated increased HER activity thanks to their high surface area and good electrical conductivity.^{69–72} Dai et al. reported the synthesis of MoS₂ nanoparticles on rGO sheets, which exhibited high HER activity with a small over-potential of ~-0.1 V, and a Tafel slope as small as 41 mV/dec because of MoS₂ particles with an abundance of catalytic edge sites and an interconnected conducting network of rGO-induced efficient hydrogen evolution.⁶⁹ Similarly, Liu et al. synthesized MoS₂ nanoparticles on mesoporous graphene foams (MoS₂/MGFs) combining high specific surface area and an interconnected conductive graphene skeleton.⁷⁰ The MoS₂/MGF hybrid exhibited excellent electrocatalytic activity for HER with a Tafel slope of 42 mV/dec.

Merki et al. also hypothesized that the edge activity is related to the unsaturated S atom.⁷³ Amorphous MoS₂ has defects and unsaturated S atoms, which can contribute to the evolution of H₂.^{73,74} Hu et al. reported that amorphous MoS₃ has more unsaturated S atoms than crystalline MoS₂.⁷⁴ The amorphous MoS₃ particles exhibited highly electrocatalytic HER with a Tafel slope of 41 mV/dec. They claimed that the unsaturated S atoms in amorphous MoS₃ can form S-H bonds that facilitate H₂ evolution. Recently, Li et al. grew graphene on a 3D Ni foam, and then synthesized MoS₂ on the surface through thermolysis of (NH₄)₂MoS₄ at 100–300°C.⁷⁵ Interestingly, the amorphous MoS_x obtained at lower growth temperatures of 120°C showed the best electrocatalytic activity with an onset potential of -0.141 to -0.109 V versus RHE and a Tafel slope of ~43 mV/dec. They explained that the higher HER activity was related to the presence of bridging S₂²⁻ or apical S²⁻ in the amorphous state. The importance of crystallinity on the HER

activity of MoS₂ and WS₂ has been investigated.⁷⁶ Note that amorphous MoS₂ on carbon cloth exhibited higher activity than crystalline MoS₂, whereas WS₂ gave the opposite result. The exact reason for the higher activity of crystalline WS₂ as compared to amorphous WS₂ has not yet been determined.⁷⁶

1T MoS₂ and WS₂ sheets for HER

Jin et al. reported a comparison of HER activities between 2H and 1T MoS₂ sheets.²⁸ Flower-like MoS₂ sheets with a high density of exposed edges were grown using chemical vapor deposition (**Figure 3b**).²⁸ The as-grown 2H MoS₂ sheets were converted to 1T MoS₂ sheets by treating them in a *n*-butyllithium solution. The 1T MoS₂ sheets showed improved HER activity with a Tafel slope of 43 mV/dec, compared to the 2H MoS₂ sheets with a Tafel slope of 110 mV/dec. This is because the metallic 1T MoS₂ sheets exhibit a decreased charge-transfer resistance relative to the as-grown 2H MoS₂.

Zhang et al. reported the catalytic activity of 1T phase MoS₂ sheets decorated with metal nanoparticles (Pt-, Pd-, and Ag-MoS₂) for HER.⁷⁷ The 1T phase MoS₂ and Pt decorated MoS₂ sheets showed a Tafel slope of 94 and 40 mV/dec, respectively. Chhowalla et al. studied the influence of strain in the 1T phase on the catalytic activity (**Figure 3c**).¹⁵ Chemically exfoliated WS₂ sheets have a high proportion of strained metallic 1T phase and thus show high HER performance with a Tafel slope of 60 mV/dec. 2H WS₂ shows poor HER activity; however, its hybrid form with rGO can be a promising catalyst because the WS₂/rGO showed a low over-potential and a Tafel slope of 58 mV/dec.⁷²

HER of pyrite TMDs

CoS₂ has been investigated as a promising HER catalyst. CoS₂ films synthesized by gas-phase reactions showed an over-potential of -180 mV and a Tafel slope of 44.6 mV/dec.^{78,79} CoS₂ micro- and nanowires have over-potentials of ~-100 mV and -70 mV, respectively, and Tafel slopes of 58 mV/dec and 51.6 mV/dec, respectively.⁷⁸ Recently, CoS₂ was synthesized on a large scale by adding GO of sufficient quantity (at least 2 mg/mL) via the hydrothermal method.⁸⁰ The resulting CoS₂/rGO hybrid exhibited high electrocatalytic activity with a Tafel slope of 48 mV/dec. In addition, the family of the pyrite phase, including NiS₂, FeS₂, and CoSe₂, also exhibited high activity for HER (**Figure 3d**).^{79,81–83}

Metallic 1T phase TMDs as electrodes in field-effect transistors

The finite and direct bandgap in single-layer TMDs make them particularly useful for logic devices.^{84–87} However, despite the fact that the effective masses of the conduction and valence band edges have been calculated to be rather symmetric (an electron effective mass ~0.57 and a hole effective mass ~0.66), the MoS₂ field-effect transistors exhibit *n*-type characteristics due to large injection barriers for holes and impractically high contact resistance (kΩ).^{88–90} Thus a major challenge in single-layer TMD electronics is in the formation of Ohmic contacts

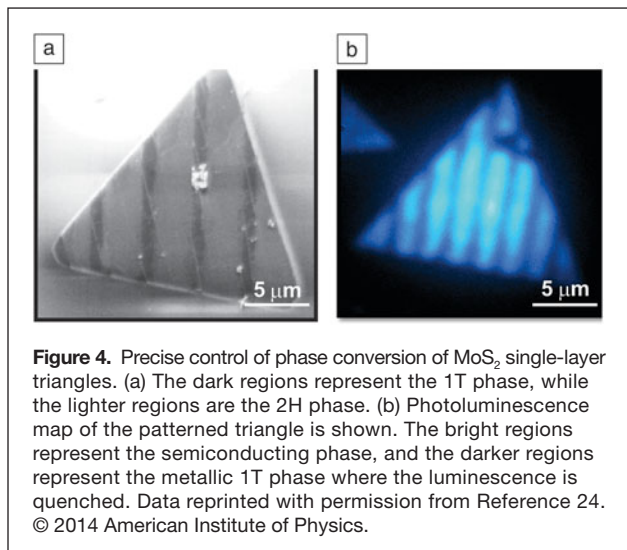


Figure 4. Precise control of phase conversion of MoS₂ single-layer triangles. (a) The dark regions represent the 1T phase, while the lighter regions are the 2H phase. (b) Photoluminescence map of the patterned triangle is shown. The bright regions represent the semiconducting phase, and the darker regions represent the metallic 1T phase where the luminescence is quenched. Data reprinted with permission from Reference 24. © 2014 American Institute of Physics.

to the individual layers. To this end, graphene has been used as an effective low barrier contact.^{91–93}

However, the lack of work function matching leads to Schottky junctions at the contacts. One way to overcome this is to utilize the metallic 1T phase of TMDs for contacts. Chhowalla et al. recently demonstrated that the interface between the 2H and 1T phases is structurally coherent.⁴ It has also been demonstrated that it is possible to convert the 2H nanosheets to the 1T phase with fine control and precision by exposing them to *n*-butyllithium or lithium boron hydride. Patterning of the 1T and 2H phases on the same TMD nanosheet allows the realization of lateral heterostructures such as those shown in **Figure 4** that are useful for devices.^{23,24} Using the 1T phase as the source and drain electrodes while keeping the 2H phase as the channel, it is possible to fabricate devices with contact resistance values of ~200–300 Ω-μm.²³ The low contact resistance facilitates charge injection and collection at the electrodes and improves the performance of the devices.

Conclusion

Exfoliated TMDs are interesting for both fundamental and technologically relevant research. In addition to their chemical versatility, the ability to engineer their phases is an additional variable that can be used to tune their properties. Phase engineering offers unique opportunities for studying and realizing novel phenomena in 2D TMDs.

References

1. M. Py, R. Haering, *Can. J. Phys.* **61**, 76 (1983).
2. P. Joensen, R. Frindt, S.R. Morrison, *Mater. Res. Bull.* **21**, 457 (1986).
3. J. Heising, M.G. Kanatzidis, *J. Am. Chem. Soc.* **121**, 638 (1999).
4. G. Eda, T. Fujita, H. Yamaguchi, D. Voiry, M. Chen, M. Chhowalla, *ACS Nano* **6**, 7311 (2012).
5. G. Eda, H. Yamaguchi, D. Voiry, T. Fujita, M. Chen, M. Chhowalla, *Nano Lett.* **11**, 5111 (2011).
6. X. Qian, J. Liu, L. Fu, J. Li, *Science* **346**, 1344 (2014).
7. B. Schönfeld, J. Huang, S. Moss, *Acta Crystallogr. B Struct. Sci.* **39**, 404 (1983).

8. M. Calandra, *Phys. Rev. B Condens. Matter* **88**, 245428 (2013).
9. M. Kan, J. Wang, X. Li, S. Zhang, Y. Li, Y. Kawazoe, Q. Sun, P. Jena, *J. Phys. Chem. C* **118**, 1515 (2014).
10. H.-L. Tsai, J. Heising, J.L. Schindler, C.R. Kannewurf, M.G. Kanatzidis, *Chem. Mater.* **9**, 879 (1997).
11. D. Yang, R. Frindt, *J. Phys. Chem. Solids* **57**, 1113 (1996).
12. J. Heising, M.G. Kanatzidis, *J. Am. Chem. Soc.* **121**, 11720 (1999).
13. P. Joensen, E. Crozier, N. Alberding, R. Frindt, *J. Phys. C Solid State Phys.* **20**, 4043 (1987).
14. S.J. Sandoval, D. Yang, R. Frindt, J. Irwin, *Phys. Rev. B Condens. Matter* **44**, 3955 (1991).
15. D. Voiry, H. Yamaguchi, J. Li, R. Silva, D.C. Alves, T. Fujita, M. Chen, T. Asefa, V.B. Shenoy, G. Eda, *Nat. Mater.* **12**, 850 (2013).
16. A.N. Enyashin, G. Seifert, *Comput. Theor. Chem.* **999**, 13 (2012).
17. Y. Cheng, A. Nie, Q. Zhang, L.-Y. Gan, R. Shahbazian-Yassar, U. Schwingenschlogl, *ACS Nano* **8**, 11447 (2014).
18. A.N. Enyashin, L. Yadgarov, L. Houben, I. Popov, M. Weidenbach, R. Tenne, M. Bar-Sadan, G. Seifert, *J. Phys. Chem. C* **115**, 24586 (2011).
19. Y.-C. Lin, D.O. Dumcenco, Y.-S. Huang, K. Suenaga, *Nat. Nanotechnol.* **9**, 391 (2014).
20. L. Wang, Z. Xu, W. Wang, X. Bai, *J. Am. Chem. Soc.* **136**, 6693 (2014).
21. Y. Kang, S. Najmaei, Z. Liu, Y. Bao, Y. Wang, X. Zhu, N.J. Halas, P. Nordlander, P.M. Ajayan, J. Lou, *Adv. Mater.* **26**, 6467 (2014).
22. K.-A.N. Duerloo, Y. Li, E.J. Reed, *Nat. Commun.* **5**, 4214 (2014).
23. R. Kappera, D. Voiry, S.E. Yalcin, B. Branch, G. Gupta, A.D. Mohite, M. Chhowalla, *Nat. Mater.* **13**, 1128 (2014).
24. R. Kappera, D. Voiry, S.E. Yalcin, W. Jen, M. Acerce, S. Torrel, B. Branch, S. Lei, W. Chen, S. Najmaei, *APL Mater.* **2**, 092516 (2014).
25. D. Voiry, M. Salehi, R. Silva, T. Fujita, M. Chen, T. Asefa, V.B. Shenoy, G. Eda, M. Chhowalla, *Nano Lett.* **13**, 6222 (2013).
26. Y. Iwasa, J. Ye, Y. Zhang, *Science* **338**, 1193 (2012).
27. N.F. Yuan, K.F. Mak, K. Law, *Phys. Rev. Lett.* **113**, 097001 (2014).
28. M.A. Lukowski, A.S. Daniel, F. Meng, A. Forticaux, L. Li, S. Jin, *J. Am. Chem. Soc.* **135**, 10274 (2013).
29. B. Mahler, V. Hoepfner, K. Liao, G.A. Ozin, *J. Am. Chem. Soc.* **136**, 14121 (2014).
30. U. Maitra, U. Gupta, M. De, R. Datta, A. Govindaraj, C. Rao, *Angew. Chem. Int. Ed.* **52**, 13057 (2013).
31. H. Wang, Z. Lu, S. Xu, D. Kong, J.J. Cha, G. Zheng, P.-C. Hsu, K. Yan, D. Bradshaw, F.B. Prinz, Y. Cui, *Proc. Natl. Acad. Sci. U.S.A.* **110**, 19701 (2013).
32. M.S. Whittingham, F.R. Gamble, *Mater. Res. Bull.* **10**, 363 (1975).
33. M.B. Dines, *Mater. Res. Bull.* **10**, 287 (1975).
34. Y. Liang, R. Feng, S. Yang, H. Ma, J. Liang, J. Chen, *Adv. Mater.* **23**, 640 (2011).
35. J. Xiao, D. Choi, L. Cosimbescu, P. Koech, J. Liu, J.P. Lemmon, *Chem. Mater.* **22**, 4522 (2010).
36. G.S. Bang, K.W. Nam, J.Y. Kim, J. Shin, J.W. Choi, S.-Y. Choi, *ACS Appl. Mater. Interfaces* **6**, 7084 (2014).
37. K. Chang, W. Chen, *ACS Nano* **5**, 4720 (2011).
38. H. Hwang, H. Kim, J. Cho, *Nano Lett.* **11**, 4826 (2011).
39. M.R. Lukatskaya, O. Mashtalir, C.E. Ren, Y. Dall'Agnese, P. Rozier, P.L. Taberna, M. Naguib, P. Simon, M.W. Barsoum, Y. Gogotsi, *Science* **341**, 1502 (2013).
40. O. Mashtalir, M. Naguib, V.N. Mochalin, Y. Dall'Agnese, M. Heon, M.W. Barsoum, Y. Gogotsi, *Nat. Commun.* **4**, 1716 (2013).
41. M. Naguib, M. Kurtoglu, V. Presser, J. Lu, J. Niu, M. Heon, L. Hultman, Y. Gogotsi, M.W. Barsoum, *Adv. Mater.* **23**, 4248 (2011).
42. M. Naguib, O. Mashtalir, J. Carle, V. Presser, J. Lu, L. Hultman, Y. Gogotsi, M.W. Barsoum, *ACS Nano* **6**, 1322 (2012).
43. M. Naguib, V.N. Mochalin, M.W. Barsoum, Y. Gogotsi, *Adv. Mater.* **26**, 992 (2014).
44. M. Ghidui, M.R. Lukatskaya, M.-Q. Zhao, Y. Gogotsi, M.W. Barsoum, *Nature* **516**, 78 (2014).
45. L. Cao, S. Yang, W. Gao, Z. Liu, Y. Gong, L. Ma, G. Shi, S. Lei, Y. Zhang, S. Zhang, *Small* **9**, 2905 (2013).
46. J.M. Soon, K.P. Loh, *Electrochem. Solid-State Lett.* **10**, A250 (2007).
47. E.G. da Silveira Firmiano, A.C. Rabelo, C.J. Dalmaschio, A.N. Pinheiro, E.C. Pereira, W.H. Schreiner, E.R. Leite, *Adv. Energy Mater.* **4**, 1301380 (2014).
48. S. Ratha, C.S. Rout, *ACS Appl. Mater. Interfaces* **5**, 11427 (2013).
49. Z. Wang, T. Chen, W. Chen, K. Chang, L. Ma, G. Huang, D. Chen, J.Y. Lee, *J. Mater. Chem. A* **1**, 2202 (2013).
50. X. Cao, Y. Shi, W. Shi, X. Rui, Q. Yan, J. Kong, H. Zhang, *Small* **9**, 3433 (2013).
51. L. David, R. Bhandavat, G. Singh, *ACS Nano* **8**, 1759 (2014).
52. X. Peng, L. Peng, C. Wu, Y. Xie, *Chem. Soc. Rev.* **43**, 3303 (2014).
53. B. Luo, Y. Fang, B. Wang, J. Zhou, H. Song, L. Zhi, *Energy Environ. Sci.* **5**, 5226 (2012).
54. X. Wang, X. Shen, Z. Wang, R. Yu, L. Chen, *ACS Nano* **8**, 11394 (2014).

55. M. Mortazavi, C. Wang, J. Deng, V.B. Shenoy, N.V. Medhekar, *J. Power Sources* **268**, 279 (2014).
56. Y.-X. Wang, K.H. Seng, S.-L. Chou, J.-Z. Wang, Z. Guo, D. Wexler, H.-K. Liu, S.-X. Dou, *Chem. Commun.* **50**, 10730 (2014).
57. B.L. Ellis, L.F. Nazar, *Curr. Opin. Solid State Mater. Sci.* **16**, 168 (2012).
58. M. Acerce, D. Voiry, M. Chhowalla, *Nat. Nanotechnol.* **10**, 313 (2015).
59. J. Feng, X. Sun, C. Wu, L. Peng, C. Lin, S. Hu, J. Yang, Y. Xie, *J. Am. Chem. Soc.* **133**, 17832 (2011).
60. H. Tributsch, J. Bennett, *J. Electroanal. Chem. Interfacial Electrochem.* **81**, 97 (1977).
61. H. Tributsch, *Ber. Bunsenges Phys. Chem.* **81**, 361 (1977).
62. B. Hinnemann, P.G. Moses, J. Bonde, K.P. Jørgensen, J.H. Nielsen, S. Hørch, I. Chorkendorff, J.K. Nørskov, *J. Am. Chem. Soc.* **127**, 5308 (2005).
63. T.F. Jaramillo, K.P. Jørgensen, J. Bonde, J.H. Nielsen, S. Hørch, I. Chorkendorff, *Science* **317**, 100 (2007).
64. J. Bonde, P.G. Moses, T.F. Jaramillo, J.K. Nørskov, I. Chorkendorff, *Faraday Discuss.* **140**, 219 (2009).
65. D. Merki, H. Vrubel, L. Rovelli, S. Fierro, X. Hu, *Chem. Sci.* **3**, 2515 (2012).
66. J. Kibsgaard, Z. Chen, B.N. Reinecke, T.F. Jaramillo, *Nat. Mater.* **11**, 963 (2012).
67. D. Kong, H. Wang, J.J. Cha, M. Pasta, K.J. Koski, J. Yao, Y. Cui, *Nano Lett.* **13**, 1341 (2013).
68. Z. Chen, D. Cummins, B.N. Reinecke, E. Clark, M.K. Sunkara, T.F. Jaramillo, *Nano Lett.* **11**, 4168 (2011).
69. Y. Li, H. Wang, L. Xie, Y. Liang, G. Hong, H. Dai, *J. Am. Chem. Soc.* **133**, 7296 (2011).
70. L. Liao, J. Zhu, X. Bian, L. Zhu, M.D. Scanlon, H.H. Girault, B. Liu, *Adv. Funct. Mater.* **23**, 5326 (2013).
71. E.G. Firmiano, M.A. Cordeiro, A.C. Rabelo, C.J. Dalmaschio, A.N. Pinheiro, E.C. Pereira, E.R. Leite, *Chem. Commun.* **48**, 7687 (2012).
72. J. Yang, D. Voiry, S.J. Ahn, D. Kang, A.Y. Kim, M. Chhowalla, H.S. Shin, *Angew. Chem. Int. Ed.* **52**, 13751 (2013).
73. D. Merki, S. Fierro, H. Vrubel, X. Hu, *Chem. Sci.* **2**, 1262 (2011).
74. H. Vrubel, D. Merki, X. Hu, *Energy Environ. Sci.* **5**, 6136 (2012).
75. Y.H. Chang, C.T. Lin, T.Y. Chen, C.L. Hsu, Y.H. Lee, W. Zhang, K.H. Wei, L.J. Li, *Adv. Mater.* **25**, 756 (2013).
76. T.-Y. Chen, Y.-H. Chang, C.-L. Hsu, K.-H. Wei, C.-Y. Chiang, L.-J. Li, *Int. J. Hydrogen Energy* **38**, 12302 (2013).
77. X. Huang, Z. Zeng, S. Bao, M. Wang, X. Qi, Z. Fan, H. Zhang, *Nat. Commun.* **4**, 1444 (2013).
78. M.S. Faber, R. Dziedzic, M.A. Lukowski, N.S. Kaiser, Q. Ding, S. Jin, *J. Am. Chem. Soc.* **136**, 10053 (2014).
79. M.S. Faber, M.A. Lukowski, Q. Ding, N.S. Kaiser, S. Jin, *J. Phys. Chem. C* **118**, 21347 (2014).
80. S. Peng, L. Li, X. Han, W. Sun, M. Srinivasan, S.G. Mhaisalkar, F. Cheng, Q. Yan, J. Chen, S. Ramakrishna, *Angew. Chem. Int. Ed.* **53**, 12594 (2014).
81. D.-Y. Wang, M. Gong, H.-L. Chou, C.-J. Pan, H.-A. Chen, Y. Wu, M.-C. Lin, M. Guan, J. Yang, C.-W. Chen, *J. Am. Chem. Soc.* **137**, 1587 (2015).
82. C. Tang, Z. Pu, Q. Liu, A.M. Asiri, X. Sun, *Electrochim. Acta* **153**, 508 (2015).
83. D. Kong, J.J. Cha, H. Wang, H.R. Lee, Y. Cui, *Energy Environ. Sci.* **6**, 3553 (2013).
84. H.-Y. Chang, S. Yang, J. Lee, L. Tao, W.-S. Hwang, D. Jena, N. Lu, D. Akinwande, *ACS Nano* **7**, 5446 (2013).
85. S. Das, H.-Y. Chen, A.V. Penumatcha, J. Appenzeller, *Nano Lett.* **13**, 100 (2012).
86. B. Radisavljevic, A. Radenovic, J. Brivio, V. Giacometti, A. Kis, *Nat. Nanotechnol.* **6**, 147 (2011).
87. H. Wang, L. Yu, Y.-H. Lee, Y. Shi, A. Hsu, M.L. Chin, L.-J. Li, M. Dubey, J. Kong, T. Palacios, *Nano Lett.* **12**, 4674 (2012).
88. Y. Yoon, K. Ganapathi, S. Salahuddin, *Nano Lett.* **11**, 3768 (2011).
89. S. Kim, A. Konar, W.-S. Hwang, J.H. Lee, J. Lee, J. Yang, C. Jung, H. Kim, J.-B. Yoo, J.-Y. Choi, *Nat. Commun.* **3**, 1011 (2012).
90. H. Peelaers, C.G. Van de Walle, *Phys. Rev. B Condens. Matter* **86**, 241401 (2012).
91. L. Yu, Y.-H. Lee, X. Ling, E.J.G. Santos, Y.C. Shin, Y. Lin, M. Dubey, E. Kaxiras, J. Kong, H. Wang, T. Palacios, *Nano Lett.* **14**, 3055 (2014).
92. T. Roy, M. Tosun, J.S. Kang, A.B. Sachid, S.B. Desai, M. Hettick, C.C. Hu, A. Javey, *ACS Nano* **8**, 6259 (2014).
93. Y.T. Lee, K. Choi, H.S. Lee, S.W. Min, P.J. Jeon, D.K. Hwang, H.J. Choi, S. Im, *Small* **10**, 2356 (2014). □

Upper left photo by Alexandra Stein, courtesy of NISE Network.

MRS
MATERIALS RESEARCH SOCIETY
FOUNDATION

give to the
causes you
care about

**Education
& Outreach**

**University
Chapters**

Awards

Make the most of your giving at www.mrs.org/foundation.